Digestive Diseases and Sciences
https://doi.org/10.1007/s10620-023-08079-w

ORIGINAL ARTICLE

Power-Controlled, Irrigated Radio-Frequency Ablation of Gastric Tissue: A Biophysical Analysis of Lesion Formation

Ashton Matthee[1] · Zahra Aghababaie[1] · Sam Simmonds[1] · Jarrah M. Dowrick[1] · Linley A. Nisbet[1] · Gregory B. Sands[1] · Timothy R. Angeli-Gordon[1,2]

Received: 27 April 2023 / Accepted: 4 August 2023

Abstract

Background Radio-frequency ablation of gastric tissue is in its infancy compared to its extensive history and use in the cardiac field.

Aims We employed power-controlled, irrigated radio-frequency ablation to create lesions on the serosal surface of the stomach to examine the impact of ablation power, irrigation, temperature, and impedance on lesion formation and tissue damage.

Methods A total of 160 lesions were created in vivo in female weaner pigs ($n=5$) using a combination of four power levels (10, 15, 20, 30 W) at two irrigation rates (2, 5 mL min^{-1}) and with one temperature-controlled (65 °C) reference setting previously validated for electrophysiological intervention in the stomach.

Results Power and irrigation rate combinations above 15 W resulted in lesions with significantly higher surface area and depth than the temperature-controlled setting. Irrigation resulted in significantly lower temperature ($p<0.001$) and impedance ($p<0.001$) compared to the temperature-controlled setting. No instances of perforation or tissue pop were recorded for any ablation sequence.

Conclusion Power-controlled, irrigated radio-frequency ablation of gastric tissue is effective in creating larger and deeper lesions at reduced temperatures than previously investigated temperature-controlled radio-frequency ablation, highlighting a substantial improvement. These data define the biophysical impact of ablation parameters in gastric tissue, and they will guide future translation toward clinical application and in silico gastric ablation modeling.

✉ Timothy R. Angeli-Gordon
t.angeli@auckland.ac.nz

[1] Auckland Bioengineering Institute, University of Auckland, Private Bag, 92019 Auckland, New Zealand

[2] Department of Surgery, University of Auckland, Auckland, New Zealand

Published online: 16 August 2023

Graphical Abstract

Combination of ablation settings (10–30 W power, 2–5 mL min^{-1} irrigation) were used to create serosal spot lesions. Histological analysis of lesions quantified localized tissue damage.

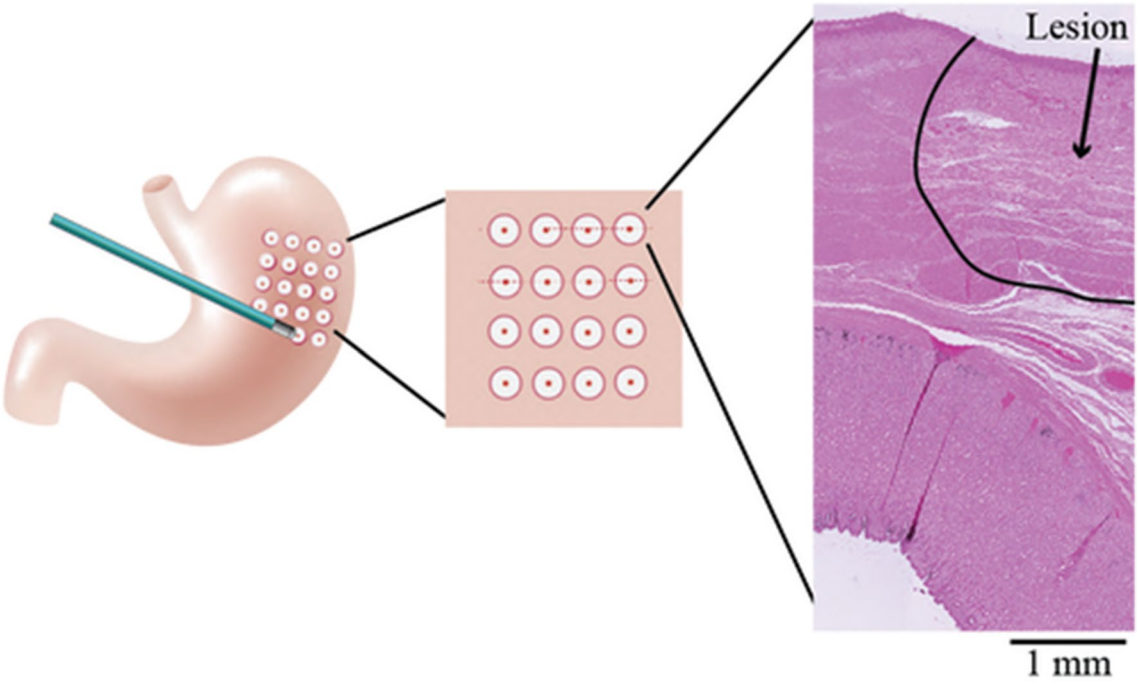

Keywords Gastrointestinal · Stomach · Electrophysiology · Radio-frequency ablation · Catheter ablation

Abbreviations

H&E	Hematoxylin and eosin
ICC	Interstitial cells of Cajal
PC-I	Power-controlled, irrigated
RFA	Radio-frequency ablation
SD	Standard deviation
TC	Temperature-controlled
TDS	Tissue damage score

Introduction

Radio-frequency ablation (RFA) is a common form of thermal ablation used electrophysiologically to correct cardiac arrhythmias through the destruction of abnormally active tissue [1, 2]. Structurally, RFA is also used in the management and treatment of both benign and malignant tumors of the liver, kidney, bone, and lung [3]. Within the field of gastroenterology, RFA has been used to treat a variety of conditions, including gastric antral vascular ectasia [4], Barrett's esophagus with dysplasia [5], and malignant biliary obstructions [6]. Applying a high-frequency (300 kHz to 700 kHz) alternating electric current results in resistive or Joule heating of the tissue [7, 8]. This heating is most intense at the contact interface and thermally conducts further into the tissue [7, 8]. If the tissue temperature is maintained above approximately 60 °C for a sufficient period, it causes irreversible damage, known as a lesion [9]. Higher temperatures are not necessarily beneficial. Tissue temperatures over 100 °C commonly result in coagulated plasma on the catheter tip leading to a rise in electrical impedance, preventing effective delivery of current, and causing tissue charring [10]. Excessive heating may result in tissue fluid vaporization leading to audible steam 'pops' or perforation, which is the most serious potential complication of ablation [11, 12]. Although the principles of ablation are the same for all of its uses, the electrodes, power delivery, and ablation target differ.

When ablation is used to target abnormally-conducting heart tissue, the non-conducting lesion that is created prevents electrical conduction through this region and enables normal cardiac electrical activity to resume [13, 14]. Lesion size is proportional to many parameters, including increased tissue temperature, power delivery (energy dose), duration, and contact force [15–17]. The challenge with RFA as a clinical therapy is ensuring the sufficient destruction of arrhythmic tissue to prevent recurrence, while maintaining the mechanical integrity of the tissue [18, 19]. However,

recurrences due to incomplete ablation are relatively common in cardiac applications [19, 20]. Innovations and developments in RFA technology have sought to make ablation as efficient as possible while reducing the chance of forming an incomplete or ineffective lesion. Irrigation is one such innovation where liquid flowing through the ablation catheter acts as a heat sink, cooling the catheter–tissue interface and preventing impedance rise. Irrigation enables increased energy dose through more consistent power delivery without increasing the risk of coagulation formation, which improves ablation efficiency and efficacy, and results in larger lesion size [16, 21]. With irrigated ablation, power is typically delivered at a constant level, which is known as power-controlled, irrigated (PC-I) ablation. In comparison, standard catheter ablation uses a non-irrigated catheter that delivers varying power to achieve a set temperature [8].

The use of RFA for gastric ablation is still in its infancy compared to its use for cardiac ablation. This study aimed to improve our understanding of the biophysics of gastric RFA from an electrophysiological motivation. Similar to the heart, stomach motility is controlled, in part, through electrophysiological events known as slow waves. Abnormal slow-wave activity has been associated with gastric motility disorders, including functional dyspepsia, gastroparesis, and chronic unexpected nausea and vomiting [22–24]. Slow waves are conducted through gastric tissue by a network of interconnected Interstitial Cells of Cajal (ICCs), electrically active cells located between and within the muscle layers of the stomach [25]. Studies by Aghababaie et al. have progressed gastric ablation from proof-of-concept to recovery (two-week, porcine model) studies [26–28]. These studies have demonstrated RFA as a promising emerging method for the modulation of slow-wave activity through the disruption of the ICC network, eliminating ectopic pacemakers responsible for causing dysrhythmic activity and restoring normal slow-wave propagation patterns [26–28]. Despite the success of the studies, they were limited to a small range of settings using only temperature-controlled (TC) ablation.

In this study, PC-I RFA was applied to the porcine gastric serosal surface in vivo with various power settings and irrigation rates. Lesion surface area, temperature, and tissue damage were quantified to inform the relationships between these settings and indicate suitable ranges for safe and effective gastric ablation.

Methods

Animal Preparation

All procedures were approved by the University of Auckland Animal Ethics Committee (approval AEC3090) and conformed to the Guiding Principles for Research Involving Animals and Human Beings. Experiments were performed in vivo with female crossbreed weaner pigs ($n = 5$, 43.1 ± 2.2 kg). Animal care has been previously described in detail [29]. Anesthesia was induced with Zoletil and maintained with either isoflurane ($n = 3$; 2.5–5% with an oxygen flow of 400 mL min^{-1} within a closed system) or propofol ($n = 2$; Diprivan 2%, 0.2–0.4 mg kg^{-1} min^{-1}; AstraZeneca, UK). Vital signs, including heart rate, blood pressure, and temperature, were continuously monitored and remained within normal physiological ranges throughout the studies. A midline laparotomy was performed to access the serosal surface of the stomach. At the conclusion of the experiment, animals were euthanized with an intravenous injection of sodium pentobarbital.

Radio-Frequency Ablation

A cardiac ablation system with a Stokert-70 RF generator (Biosense Webster, Irvine, CA, USA) was used to perform RFA on the serosal surface of the stomach using combinations of four power-controlled settings (10, 15, 20, 30 W) and two irrigation rates (2, 5 mL min^{-1}) via a catheter (ThermoCool; Biosense Webster, Irvine, CA, USA) irrigated with room-temperature saline (Baxter Healthcare, NSW, Australia). A reference TC ablation was also performed at 65 °C using a non-irrigated catheter, as this setting has routinely resulted in a gastric electrical conduction block [26, 27]. A sequence of four ablations spaced approximately 10 mm apart were performed for each setting (10 s per point). Ablations were performed across the stomach from greater to lesser curvature, and sequences progressed distally from the upper corpus toward the lower corpus, with each subsequent sequence approximately 15 mm distal from the previous one (Fig. 1A).

During each ablation sequence, the RF generator was monitored. Power output, catheter tip temperature, and impedance were sampled once per second over the 10-s sequence and reported as mean values.

Gross Image Evaluation

Immediately before euthanasia, the region of stomach tissue containing all of the ablated lesions was excised for gross image analysis and histological evaluation. The excised tissue sections were washed in saline, and both surfaces were photographed using a digital camera (Fig. 1B). The outline of each visible lesion on the serosal surface was manually traced using ImageJ software [30], where the lesion boundary was defined by the change in color from pink (healthy) to white (lesion). The same investigator performed all measurements to ensure consistency of the manual segmentation. Lesion surface area

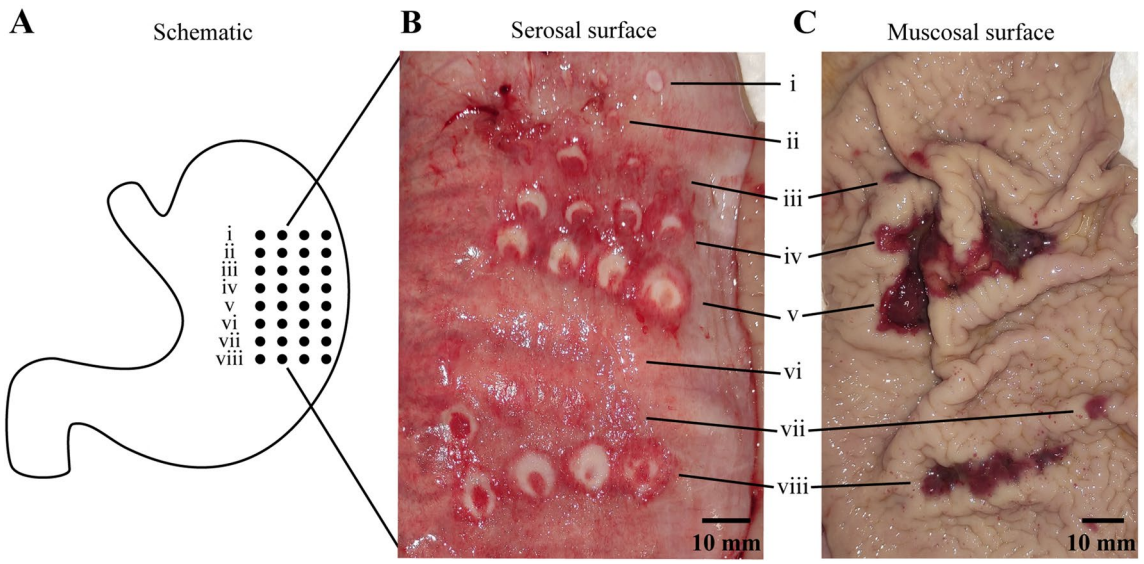

Fig. 1 Four repetitions of eight ablation settings. **A** Schematic showing grid location of ablation points on the stomach. **B** Gross image of the serosal surface following excision. **C** Gross image of the mucosal surface of the same section as B. The settings (i–viii) were as follows: (i) 65 °C at 0 mL min^{-1}; (ii) 10 W at 5 mL min^{-1}; (iii) 15 W at 5 mL min^{-1}; (iv) 20 W at 5 mL min^{-1}; (v) 30 W at 5 mL min^{-1}; (vi) 10 W at 2 mL min^{-1}; (vii) 15 W at 2 mL min^{-1}; and (viii) 20 W at 2 mL min^{-1}

was measured using the software's in-built measure tool. Lesions that were not visible were recorded as such.

Histological Analysis

Following gross imaging, the tissue was fixed in 10% neutral-buffered formalin for at least seven days. Lesions were bisected to reveal the lesion penetration profile into the tissue. Tissue sections of the bisected lesion were obtained (5 µm thick), stained with hematoxylin and eosin (H&E) [31], and digitally scanned using a high-resolution VSlide scanner (Metasystems, Altlussheim, Germany) at the Biomedical Imaging Research Unit (BIRU), University of Auckland.

The stained sections were examined for tissue structure, extravasation, and swollen nuclei, along with other markers of tissue damage, such as edema or hemorrhage. An existing scale [26] was adapted to qualitatively assess the degree of tissue damage separately for the entire muscularis and for the mucosal layer. The tissue damage score (TDS) was defined as follows: (0) no damage, all healthy tissue present; (1) minimal damage, partial damage through layer; (2) moderate damage, damage present through the entire thickness of layer; (3) excessive damage, damage entirely through layer, and tissue has lost its structure; and (4) perforation, the lesion has perforated the tissue, and the layer is no longer continuous.

Statistical Analysis

Differences in surface area, temperature, and power during ablation are expressed as mean ± standard deviation (SD). All statistical analysis was performed using R Statistical Software (v4.2.2; R Core Team 2022) [32]. Statistical differences between irrigation and power groups were determined through a one-way analysis of variance (ANOVA) model followed by a Tukey post-test with a significance threshold of $p < 0.05$. Correlations between variables were measured using the Pearson correlation coefficient (r).

Results

A total of 40 ablation sequences were performed at the various settings (PC-I: 10, 15, 20, 30 W at 2, 5 mL min^{-1} irrigation rates; TC: 65 °C, no irrigation) across five pigs ($n = 160$ spot lesions total, 20 per setting; Table 1). In all animals, RFA was applied to the serosal surface of the stomach without difficulty. There were no cases of perforation, tissue pop, or visible loss of tissue integrity during any ablation sequence. Not all settings produced lesions that were visible during gross imaging (Fig. 1B). Surface area was measured from all visible lesions (Figs. 1B, 2C), a subset of lesions were stained and imaged, and tissue damage profile was qualitatively evaluated (Table 1).

Table 1 Summary of lesion analysis and tissue damage scores

Setting	Irrigation rate (mL min^{-1})	Visible lesions (*n*/20)	Histological samples (*n*)	Muscularis score	Mucosa score
65 °C	0	13	6	1.5 ± 0.5	0 ± 0
10 W	2	8	8	1.8 ± 0.4	0.8 ± 0.8
	5	9	6	1.5 ± 0.5	1.7 ± 0.4
15 W	2	12	10	1.9 ± 0.3	0.5 ± 0.8
	5	14	10	1.7 ± 0.7	0.8 ± 0.6
20 W	2	18	15	2.1 ± 0.2	0.8 ± 0.7
	5	20	11	2.1 ± 0.5	1.4 ± 0.8
30 W	5	19	13	2.1 ± 0.5	1.6 ± 0.6

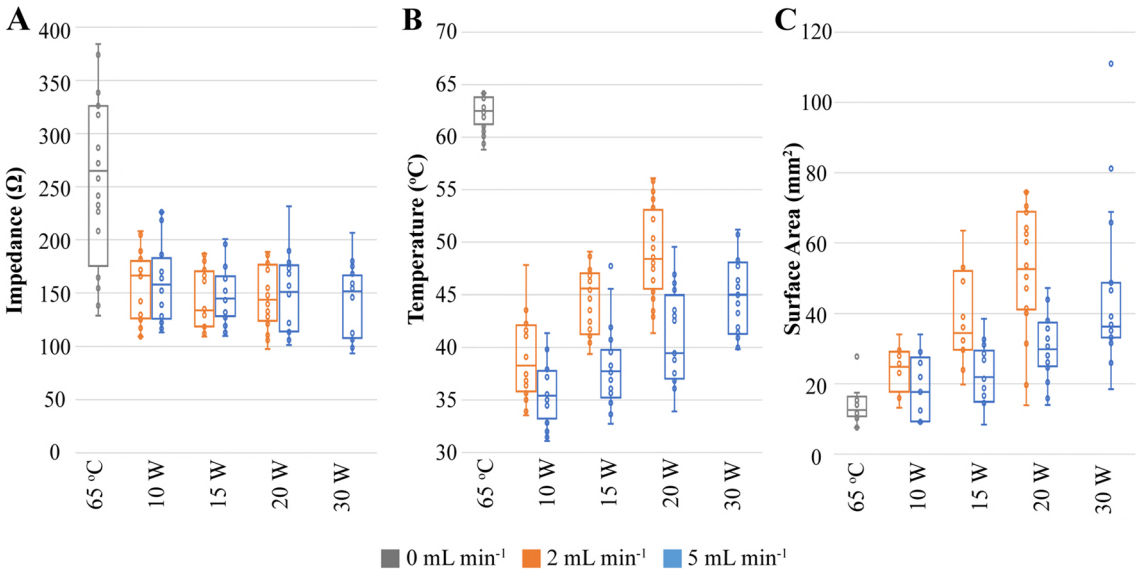

Fig. 2 Box-and-whisker plots (median, first and third quartiles, range) of **A** impedance, **B** average catheter temperature, and **C** measured surface area for each setting investigated

Gross Pathology

Upon examination of the excised tissue, lesions were identifiable by the color change from pale pink (healthy) to white or red (damaged). Visible lesions were less pronounced at lower power settings than at higher power settings. Lesions tended to appear as a white circle with an outer ring of damaged red tissue and, in some cases, had a red spot in the middle of the white section where the catheter had contacted the tissue (e.g., Fig. 1Bv, Bviii). Hematomas were observed on the mucosal surface, with the occurrence and size of a hematoma qualitatively increasing with power (Fig. 1C iv, v, viii).

Power-Controlled, Irrigated Ablation

Measures of impedance showed no significant difference for all flow rates at all power settings (Fig. 2A). The average temperature over each ablation positively correlated with the applied power setting for both irrigation rates (2 mL min^{-1}: $p < 0.001$, $r = 0.74$; 5 mL min^{-1}: $p < 0.001$, $r = 0.69$) (Fig. 2B). When comparing the two irrigation rates, temperatures for the 2 mL min^{-1} irrigation rate were higher than for 5 mL min^{-1} at all power settings, although not significantly different at 10 W (38.9 ± 3.7 °C, 35.6 ± 2.8 °C; $p = 0.06$) (Fig. 2B). There was a significant difference in temperature for the 15 W (44.6 ± 2.9 °C vs 38.2 ± 3.7 °C; $p < 0.001$) and 20 W (49.1 ± 4.3 °C vs 40 .9 ± 4.3 °C; $p < 0.001$) power settings (Fig. 2B). Lesion surface area positively correlated with power setting (2 mL min^{-1}: $p < 0.001$, $r = 0.61$; 5 mL min^{-1}: $p < 0.001$, $r = 0.56$) (Fig. 2C). The only significant difference in surface area when comparing irrigation rates was for the 20 W power setting (52.5 ± 17.4 mm^2 vs 30.4 ± 9.3 mm^2; $p < 0.001$) (Fig. 2C).

Comparison of Power-Controlled, Irrigated Versus Temperature-Controlled Ablation

TC ablation had a significantly greater impedance ($p<0.001$) than all PC-I ablations (Fig. 2A). It also had a significantly higher temperature (62.3 ± 1.6 °C) than all PC-I ablations (35–50 °C $p<0.001$) (Fig. 2B) and significantly lower power delivery (TC: 3.4 ± 2.2 W s^{-1}; PC-I: all ≥ 10 W s^{-1}) ($p<0.001$). Despite these differences, the surface area of the TC lesions was not significantly different from 10 W at 2 mL min^{-1} ($p=0.79$), 10 W at 5 mL min^{-1} ($p=0.99$), and 15 W at 5 mL min^{-1} ($p=0.80$) (Fig. 2C). The surface area of the TC lesions was significantly smaller than that of PC-I settings of 15 W at 2 mL min^{-1} ($p=0.001$), 20 W at 2 mL min^{-1} ($p<0.001$), 20 W at 5 mL min^{-1} ($p=0.04$), and 30 W at 5 mL min^{-1} ($p<0.001$) (Fig. 2C).

Temperature as a Potential Indicator of Lesion Size

To investigate whether temperature could be a potential indicator of lesion size, temperature and surface area were compared independent of power setting and separated by irrigation rate (Fig. 3). There was a significant positive correlation between temperature and surface area for both irrigation rates (2 mL min^{-1}: $p=0.04$, $r=0.34$; 5 mL min^{-1}: $p=0.003$, $r=0.37$), with no significant difference between the irrigation rates ($p=0.40$). With every degree Celsius temperature increase, the surface area increased by 1.37 mm^2 using an irrigation rate of 2 mL min^{-1} and 1.30 mm^2 using an irrigation rate of 5 mL min^{-1} (Fig. 3).

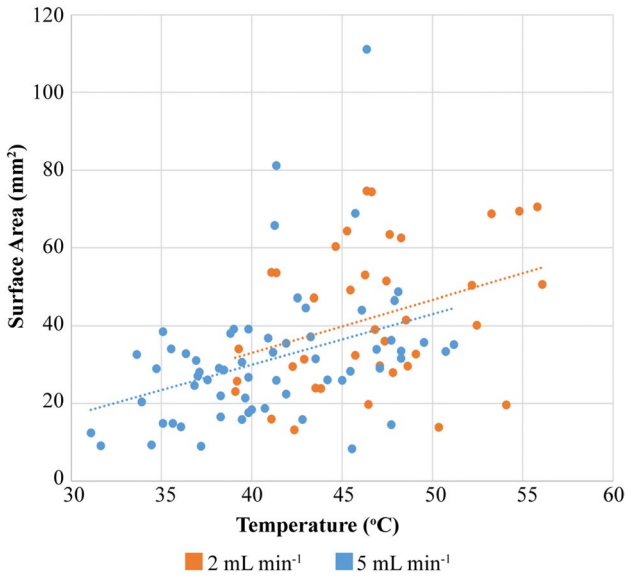

Fig. 3 Measured lesion surface area and average catheter temperature during the ablation sequence for all visible, measured lesions. Lines shown are linear least squares regression fits to data points

Histopathology

The TDS analysis is presented in Fig. 4. Qualitative analysis of H&E-stained tissue sections confirmed that lesions were localized to the ablation site, often with a clear distinction between healthy and damaged tissue (Fig. 5I). Damage was usually seen throughout the entire thickness of the gastric wall but never resulted in perforation, therefore no TDS of 4 was recorded (Fig. 4).

All ablations resulted in damage to some or all of the muscularis (TDS ≥ 1, Fig. 4), with damage identifiable by swelling and degeneration of fibers (Fig. 5II). In some PC-I cases, this damage continued deeper into the tissue to cause partial (score 1) or complete damage (score 2) to the mucosa (Fig. 4). Mucosal damage was marked by the loss of regular glandular structure and swelling (Fig. 5III). Other markers of tissue damage, such as edema and hyperemia, were seen to some degree in all samples. For 10 W, increasing the irrigation rate resulted in reduced damage to the muscularis and mucosal layers. At higher power settings (15 W and 20 W), increasing the irrigation rate caused deeper lesions with greater damage to the muscularis and mucosal layers. When the irrigation rate was constant, an increase in power resulted in deeper lesions with higher tissue damage scores (Fig. 4).

Discussion

This study presents a foundational application of PC-I RFA to gastric tissue, where PC-I settings were systematically compared to a well-established TC setting [26, 27] using various combinations of power and irrigation rates. We have demonstrated that PC-I RFA can be applied to the serosal surface of gastric tissue in vivo safely and consistently, and we have defined biophysical correlations between lesion size, damage score, temperature, and power delivery for two different irrigation rates.

We successfully applied RFA to the serosal surface of gastric tissue in vivo in all cases. Gross image analysis showed that PC-I settings created lesions with a larger surface area than the TC setting and applied power was positively related to surface area and lesion depth. Histological analysis of the lesions showed that damage to the gastric muscle layers was present in PC-I and TC ablations. All settings resulted in at least partial damage to the muscularis and, for 20 W at 2 mL min^{-1}, complete damage through the muscularis was seen in all samples. PC-I settings caused varying degrees of damage to the gastric mucosa that was not observed in TC lesions. Despite the observation of hematomas on the mucosal surface following ablation (Fig. 1C), histological analysis showed that tissue integrity was maintained (Fig. 5). No instances of perforation, coagulation, charring, or tissue

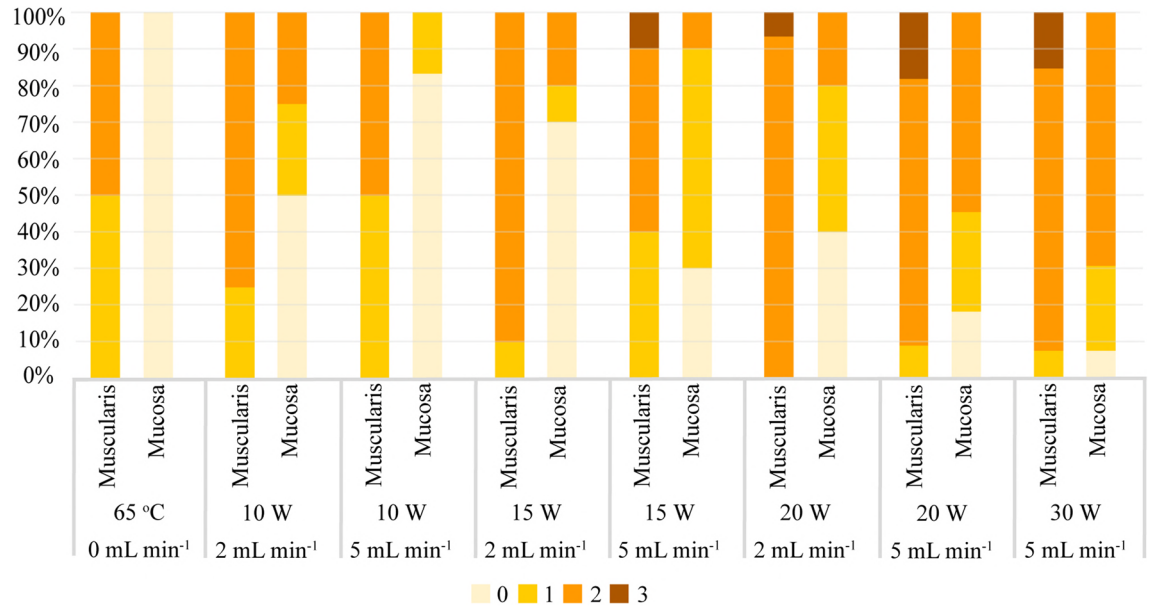

Fig. 4 Tissue damage score (TDS) proportions for each setting for the muscularis and mucosa layers. TDS: (0) no damage, all healthy tissue present; (1) minimal damage, partial damage through layer; (2) moderate damage, damage present through entire thickness of layer; (3) excessive damage, damage entirely through layer and tissue has lost its structure; and (4) perforation, tissue layer no longer continuous. Since perforation did not occur, TDS was not assessed as level 4 for any ablation sequence

pop were witnessed by the investigators during all ablation sequences. In comparison to TC, PC-I settings successfully prevented and controlled impedance rise. These findings suggest that PC-I has beneficial improvements over TC, as irrigation reduces impedance and temperature rise seen in TC RFA [12, 26], while increasing lesion depth and size. Therefore, PC-I may likely prove to be more suitable for future work in the gastric ablation field.

The 10 W power setting at 2-mL min^{-1} and 5-mL min^{-1} irrigation rates produced lesions that closely resembled the TC setting in surface area and tissue damage, although the PC-I settings tended to have more damage to the mucosa (Fig. 4). Based on these results, we hypothesize that PC-I settings will produce lesions capable of blocking slow-wave propagation, consistent with previously validated TC ablation [26, 27]. Future investigations using alternative histological protocols [33] and functional high-resolution electrical mapping can now be designed to validate and confirm this hypothesis. In order to ultimately determine which ablation procedure (PC-I vs TC) is more suitable for gastric ablation in the clinical setting, longer-term (> two weeks) recovery studies must be conducted to define the differences during the post-operative and healing phase. Alternatives to serosal ablation should also be investigated. The increased lesion depth and reduced catheter–tissue interface temperature achieved with PC-I ablation may mean that it can be successfully applied from the mucosal surface of the stomach, as irrigation would help maintain mucosal viability while the improved lesion depth would enable the deeper musculature to be targeted, disrupting the ICC network. Such an approach would enable minimally-invasive endoscopic ablation to complement emerging methods of endoscopic electrical mapping [34].

Compared to typical cardiac ablation parameters (20–50 W, 15–30 mL min^{-1}, for 30–60 s) [35–37], our study used lower power settings over shorter ablation times with significantly lower irrigation rates. The need for increased power delivery, ablation time, and irrigation rate in cardiac applications is likely due to the increased tissue thickness and enhanced energy loss associated with increased blood flow compared to gastric applications [11, 17, 38]. We report that PC-I resulted in lower temperatures than TC ablation despite a significant increase in energy dose (power), which validates the use of irrigation to decrease interface temperature while enabling increased power delivery, above what is possible with TC. Our data showed that increased power delivery is significantly correlated to increased lesion surface area for PC-I ablations, as expected (2 mL min^{-1}: $r = 0.61$; 5 mL min^{-1}: $r = 0.56$). This increased lesion size could be a useful result when translating gastric ablation toward clinical application since insufficient lesion size is a contributing factor to the recurrence of cardiac disorders [18, 19]. These relationships can also now be modeled in silico in the near term.

Many organ-specific computational models of RFA exist [39, 40], but a comprehensive model of gastric ablation does not. The data presented in this study could be used to expand existing preliminary in silico models of gastric ablation, which are currently limited to TC RFA [41], to now include PC-I

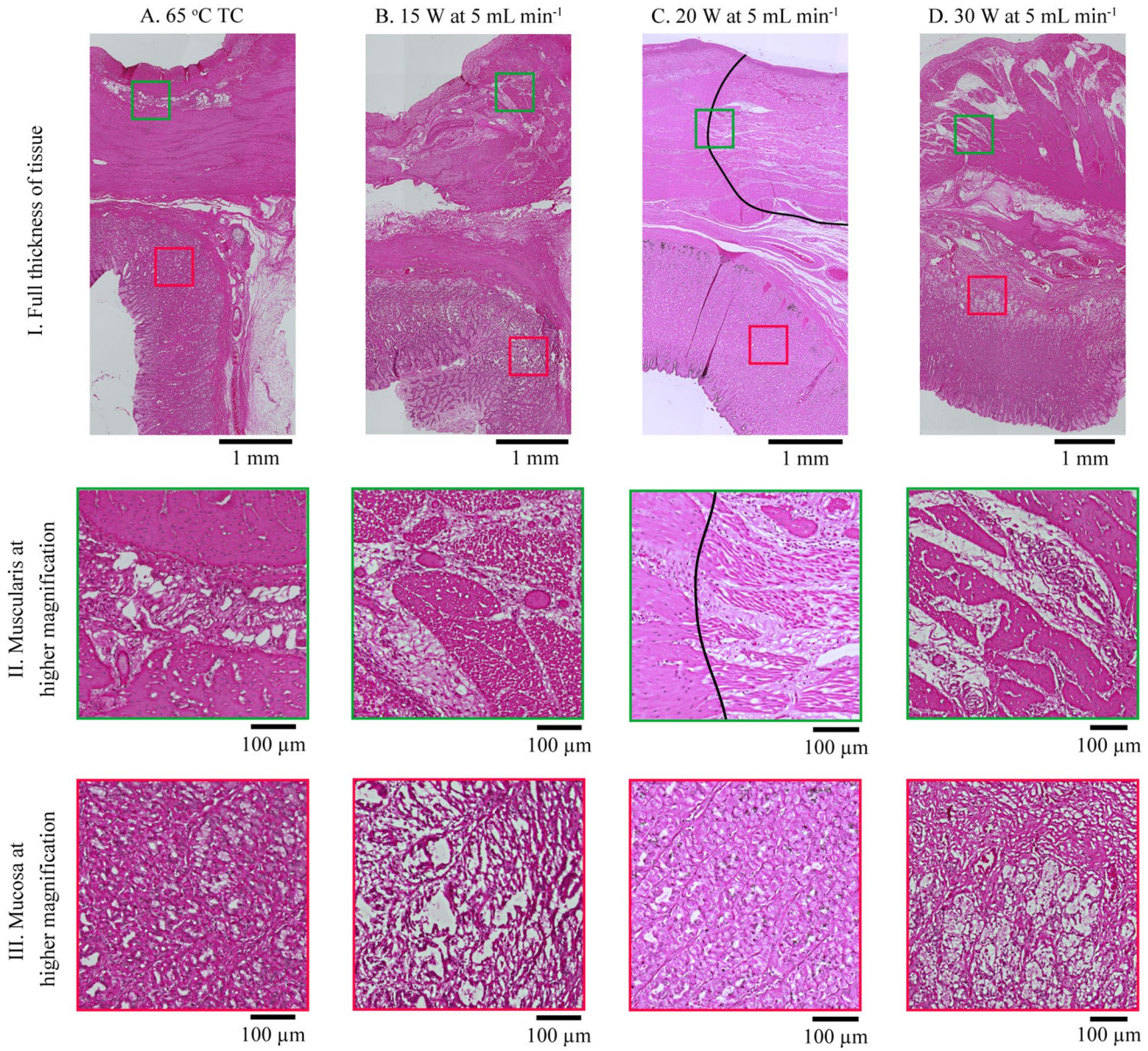

Fig. 5 Evaluation of tissue damage due to ablation using H&E stain for structural analysis. Panel I shows full-thickness tissue sections of ablated tissue. **A** 65 °C temperature-controlled; **B** 15 W at 5 mL min^{-1}; **C** 20 W at 5 mL min^{-1}, the border of the lesion is shown; and **D** 30 W at 5 mL min^{-1}. Sections of tissue indicated by the green and red boxes in panel I are shown in panels II (muscularis) and III (mucosa) at higher magnification. Tissue destruction with swollen and elongated nuclei, edema, and extravasation are identifiers of tissue damage due to ablation. All (**A**–**D**) sections present muscularis damage, while (**A**,**C**) have no mucosal damage

parameters and results. The results of the present study provide the necessary experimental data to inform such a computational model of PC-I gastric ablation. Further work in this field to create a comprehensive in silico model could be used to perform hypothesis testing of other ablation parameters that were outside of the scope of the present study. For example, the impact of contact force, catheter size, and catheter orientation could be investigated in silico, which are known to influence lesion formation [15–17, 42, 43]. Such modeling has the potential to inform best practice while reducing animal use and to serve as a bridge to first-in-human trials of gastric ablation as an electrophysiological intervention.

The biophysical relationships identified in this study may prove useful clinically, in determining the effective energy dose required to create permanent lesions in gastric tissue. It has been shown that lesions through the full thickness of the gastric muscle layers result in localized electrical conduction blocks [26], can eliminate ectopic pacemakers to restore normal propagation patterns [28], and remain safe and effective after a two-week recovery

period [27]. These results suggest that gastric ablation could be used as an intervention to eliminate abnormal slow-wave activation and/or propagation which have been associated with gastric disorders, including chronic nausea and vomiting [22], functional dyspepsia [23], and gastroparesis [24]. However, the invasiveness of gastric ablation studies for slow-wave intervention performed via open-abdomen surgery limits the applicability of this technique for routine clinical use. Performing gastric ablation from the mucosal surface via endoscopic delivery would reduce the invasiveness of the procedure. Our results demonstrate that PC-I has beneficial lesion formation compared to TC ablation and if applied from the mucosal surface, will likely aid in maintenance of mucosal integrity at the catheter–mucosa interface. The presented results also provide improved biophysical understanding of PC-I lesion formation that may aid current applications of structural ablation in the gastrointestinal field for conditions like gastric antral vascular ectasia [4], Barrett's esophagus with dysplasia [5], and malignant biliary obstructions [6].

Although best efforts were taken to standardize our experimental protocol and minimize error, some parameters known to affect lesion size, such as contact force, were not measured or explicitly controlled, which could influence our findings [42]. Our approach to evaluating tissue damage is based on qualitative assessments of the histological images obtained. A quantitative measurement, such as automated image segmentation and analysis, possibly combined with alternative stains, such as nitroblue tetrazolium, would improve the reproducibility and robustness of tissue damage evaluation in future. Improved confidence in the reliability of tissue damage evaluation may complement and validate future in silico modeling. Our investigation was limited to RFA in this study. Alternative methods of ablation, such as electroporation, have demonstrated beneficial effects in other organs, including the heart [44], prostate, pancreas, and liver [45]. Electroporation may also have beneficial effects in the stomach that could be usefully explored in future studies.

In conclusion, this study establishes a greater understanding of the biophysics of gastric PC-I RFA, defining the quantitative relationships between ablation power, temperature, irrigation rate, impedance, and lesion size, as well as assessing the qualitative tissue damage via histology in the in vivo stomach. The results demonstrate that PC-I gastric ablation offers beneficial properties of reduced impedance and interface temperature compared to TC settings while still achieving full-thickness lesion formation through the muscularis. These data can now inform the continued development and translation of gastric ablation as an interventional technique, similar to its role in interventional cardiology, where it may be able to correct abnormal slow-wave initiation observed in subsets of patients with functional dyspepsia, gastroparesis, and chronic unexplained nausea and vomiting [22–24].

Acknowledgments We thank Mrs. Satya Amirapu for her assistance and expert knowledge, the Biomedical Imaging Research Unit (BIRU), University of Auckland, for access to resources for histology imaging, and Johnson and Johnson New Zealand for their donation of the ablation equipment.

Author's contribution AM, ZA, GBS, and TRA-G contributed to conceptualization; AM, SS, LAN, and TRA-G contributed to methodology; AM, ZA, JMD, GBS, and TRA-G contributed to formal analysis and investigation; AM contributed to writing and original draft preparation; All authors contributed to writing and original draft preparation; TRA-G contributed to funding acquisition; TRA-G and GBS contributed to supervision.

Funding These studies and/or authors were supported by a Rutherford Discovery Fellowship from the Royal Society Te Apārangi and research grants from the Health Research Council New Zealand and Marsden Fund, Royal Society Te Apārangi, New Zealand. Open Access funding was enabled and organized by CAUL and its Member Institutions.

Declarations

Conflict of interest Timothy R. Angeli-Gordon is a shareholder in FlexiMap Ltd. No other authors have any conflicts of interest.

References

1. Wellens HJ. Cardiac electrophysiology: from cell to bedside. *Fourth Edition. Circulation.* 2004;110:e453–e453.
2. Soucek F, Starek Z. Use of bipolar radiofrequency catheter ablation in the treatment of cardiac arrhythmias. *Curr Cardiol Rev.* 2018;14:185–191.
3. Knavel EM, Brace CL. Tumor ablation: Common modalities and general practices. *Tech Vasc Interv Radiol.* 2013;16:192–200.
4. Dray X, Repici A, Gonzalez P et al. Radiofrequency ablation for the treatment of gastric antral vascular ectasia. *Endoscopy.* 2014;46:963–969.
5. Shaheen NJ, Overholt BF, Sampliner RE et al. Durability of radiofrequency ablation in Barrett's esophagus with dysplasia. *Gastroenterology.* 2011;141:460–468.
6. Han SY, Kim DU, Kang DH, Baek DH, Lee TH, Cho JH. Usefulness of intraductal RFA in patients with malignant biliary obstruction. *Medicine.* 2020;99:E21724.
7. Ahmed M, Brace CL, Lee FT, Goldberg SN. Principles of and advances in percutaneous ablation. *Radiology.* 2011;258:351–369.
8. Sandhu A, Nguyen DT. Forging ahead: Update on radiofrequency ablation technology and techniques. *J Cardiovasc Electrophysiol.* 2020;31:360–369.

9. Nikfarjam M, Muralidharan V, Christophi C. Mechanisms of focal heat destruction of liver tumors. *J Surg Res.* 2005;127:208–223.
10. Haines DE, Watson DD. Tissue heating during radiofrequency catheter ablation: a thermodynamic model and observations in isolated perfused and superfused canine right ventricular free wall. *Pacing Clin Electrophysiol.* 1989;12:962–976.
11. Nakagawa H, Yamanashi WS, Pitha JV et al. Comparison of in vivo tissue temperature profile and lesion geometry for radiofrequency ablation with a saline-irrigated electrode versus temperature control in a canine thigh muscle preparation. *Circulation.* 1995;91:2264–2273.
12. Haines DE, Verow AF. Observations on electrode-tissue interface temperature and effect on electrical impedance during radiofrequency ablation of ventricular myocardium. *Circulation.* 1990;82:1034–1038.
13. Morady F. Radio-frequency ablation as treatment for cardiac arrhythmias. *N Engl J Med.* 1999;340:534–544.
14. Bhatia S, Sugrue A, Asirvatham SJ. Atrial fibrillation: beyond rate control. *Mayo Clin Proc.* 2018;93:373–380.
15. Haines DE, Strunk AR, Novichenok A, Kirchhof N, Stewart M. The biophysics of passive convective cooling during catheter ablation with gold versus platinum electrodes and multielectrode phased radiofrequency energy delivery. *J Cardiovasc Electrophysiol.* 2015;26:1257–1261.
16. Weiss C, Antz M, Eick OJ, Eshagzaiy K, Meinertz T, Willems S. Radiofrequency catheter ablation using cooled electrodes: impact of irrigation flow rate and catheter contact pressure on lesion dimensions. *Pacing Clin Electrophysiol.* 2002;25:463–469.
17. Haines DE. Determinants of lesion size during radiofrequency catheter ablation: the role of electrode-tissue contact pressure and duration of energy delivery. *J Cardiovasc Electrophysiol.* 1991;2:509–515.
18. Kobza R, Hindricks G, Tanner H et al. Late recurrent arrhythmias after ablation of atrial fibrillation: incidence, mechanisms, and treatment. *Heart Rhythm.* 2004;1:676–683.
19. Langberg JJ, Calkins H, Kim YN et al. Recurrence of conduction in accessory atrioventricular connections after initially successful radiofrequency catheter ablation. *J Am Coll Cardiol.* 1992;19:1588–1592.
20. Verma A, Kilicaslan F, Pisano E et al. Response of atrial fibrillation to pulmonary vein antrum isolation is directly related to resumption and delay of pulmonary vein conduction. *Circulation.* 2005;112:627–635.
21. Yokoyama K, Nakagawa H, Wittkampf FHM. Comparison of electrode cooling between internal and open irrigation in radiofrequency ablation lesion depth and incidence of thrombus and steam pop. *Circulation.* 2006;113:11–19.
22. Angeli TR, Cheng LK, Du P et al. Loss of interstitial cells of Cajal and patterns of gastric dysrhythmia in patients with chronic unexplained nausea and vomiting. *Gastroenterology.* 2015;149:56-66.e5.
23. Gharibans AA, Coleman TP, Mousa H, Kunkel DC. Spatial patterns from high-resolution electrogastrography correlate with severity of symptoms in patients with functional dyspepsia and gastroparesis. *Clin Gastroenterol Hepatol.* 2019;17:2668–2677.
24. O'Grady G, Angeli TR, Du P et al. Abnormal initiation and conduction of slow-wave activity in gastroparesis, defined by high-resolution electrical mapping. *Gastroenterology.* 2012;143:589.
25. Farrugia G. Interstitial cells of Cajal in health and disease. *Neurogastroenterol Motil.* 2008;20:54–63.
26. Aghababaie Z, Paskaranandavadivel N, Amirapu S et al. Gastric ablation as a novel technique for modulating electrical conduction in the in vivo stomach. *Am J Physiol Gastrointest Liver Physiol.* 2021;320(4):G573–G585.
27. Aghababaie Z, O'Grady G, Nisbet LA et al. Localized bioelectrical conduction block from radiofrequency gastric ablation persists post-healing: safety and feasibility in a recovery model. *Am J Physiol Gastrointest Liver Physiol.* 2022;323:G640–G652.
28. Aghababaie Z, Cheng LK, Paskaranandavadivel N et al. Targeted ablation of gastric pacemaker sites to modulate patterns of bioelectrical slow wave activation and propagation in an anesthetized pig model. *Am J Physiol Gastrointest Liver Physiol.* 2022;322:G431–G445.
29. Angeli TR, Du P, Paskaranandavadivel N et al. The bioelectrical basis and validity of gastrointestinal extracellular slow wave recordings. *J Physiol.* 2013;591:4567–4579.
30. Schneider CA, Rasband WS, Eliceiri KW. NIH Image to ImageJ: 25 years of image analysis. *Nat Methods.* 2012;9:671–675.
31. Feldman AT, Wolfe D. Tissue processing and hematoxylin and eosin staining. *Methods Mol Biol.* 2014;1180:31–43.
32. R Core Team. R: A language and environment for statistical computing. 2022. Available from: https://www.r-project.org/
33. Yun HY, Sung R, Kim YC et al. Regional distribution of interstitial cells of Cajal (ICC) in human stomach. *Korean J Physiol Pharmacol.* 2010;14:324.
34. Angeli TR, Du P, Paskaranandavadivel N et al. High-resolution electrical mapping of porcine gastric slow-wave propagation from the mucosal surface. *Neurogastroenterol Motil.* 2017;29:e13010.
35. Guerra JM, Jorge E, Raga S et al. Effects of open-irrigated radiofrequency ablation catheter design on lesion formation and complications: in vitro comparison of 6 different devices. *J Cardiovasc Electrophysiol.* 2013;24:1157–1162.
36. Kumar S, Romero J, Stevenson WG et al. Impact of lowering irrigation flow rate on atrial lesion formation in thin atrial tissue: preliminary observations from experimental and clinical studies. *JACC Clin Electrophysiol.* 2017;3:1114–1125.
37. Müssigbrodt A, Grothoff M, Dinov B et al. Irrigated tip catheters for radiofrequency ablation in ventricular tachycardia. *Biomed Res Int.* 2015;2015:1–6.
38. Calkins H, Hindricks G, Cappato R et al. 2017 HRS/EHRA/ECAS/APHRS/SOLAECE expert consensus statement on catheter and surgical ablation of atrial fibrillation. *Heart Rhythm.* 2017;14:e275-444.
39. Macchi EG, Gallati M, Braschi G, Cigada A, Comolli L. Temperature distribution during RF ablation on ex vivo liver tissue: IR measurements and simulations. *Heat Mass Transfer.* 2015;51:611–620.
40. Jain MK, Wolf PD. Temperature-controlled and constant-power radio-frequency ablation: What affects lesion growth? *IEEE Trans Biomed Eng.* 1999;46:1405–1412.
41. Savage M, Avci R, Aghababaie Z et al. A computational model of radiofrequency ablation in the stomach, an emerging therapy for gastric dysrhythmias. *Conf Proc IEEE Eng Med Biol Soc.* 2021;2021:1495–1498.
42. Thiagalingam A, D'Avila A, Foley L et al. Importance of catheter contact force during irrigated radiofrequency ablation: evaluation in a porcine ex vivo model using a force-sensing catheter. *J Cardiovasc Electrophysiol.* 2010;21:806–811.
43. Jaïs P, Haïssaguerre M, Shah DC et al. Successful irrigated-tip catheter ablation of atrial flutter resistant to conventional radiofrequency ablation. *Circulation.* 1998;98:835–838.
44. Sugrue A, Maor E, Ivorra A et al. Irreversible electroporation for the treatment of cardiac arrhythmias. *Expert Rev Cardiovasc Ther.* 2018;16:349–360.
45. Aycock KN, Davalos RV. Irreversible electroporation: background, theory, and review of recent developments in clinical oncology. *Bioelectricity.* 2019;1:234.